Environmental Science & Technology

pubs.acs.org/est

Article

Insights into Designing Photocatalysts for Gaseous Ammonia Oxidation under Visible Light

Min Chen, Changbin Zhang,* and Hong He

Cite This: *Environ. Sci. Technol.* 2020, 54, 10544−10550

Read Online

ACCESS | Metrics & More | Article Recommendations | Supporting Information

ABSTRACT: Excessive emission of ammonia (NH_3) gives rise to a number of negative effects on the environment and human health. Photocatalysis is an efficient method to eliminate gaseous NH_3; however, photocatalytic oxidation (PCO) of NH_3 in the visible light region has not been achieved to date. Herein, we test a set of typical visible-light-sensitive photocatalysts (N-TiO_2, g-C_3N_4, and Ag_3PO_4) for NH_3 oxidation and reveal for the first time that the semiconductor Ag_3PO_4 can harness visible light to realize ambient NH_3 oxidation. Combining the activity testing results with the photochemical properties of samples, we confirm that photoexcited holes are responsible for triggering the initial key step of NH_3 oxidation (NH_3 to $^{\bullet}NH_2$), and therefore, the redox potential of photoexcited holes plays the decisive role in the reaction. We propose that an active visible light photocatalyst for NH_3 oxidation requires both a suitable band gap for visible light response and a low valence band edge associated with a high oxidation potential for activating NH_3 to $^{\bullet}NH_2$. Our findings provide new insights into the PCO of pollutants under visible light and will benefit future design of more efficient visible-light-sensitive photocatalysts.

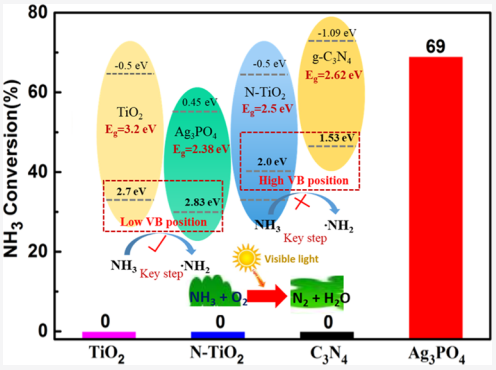

1. INTRODUCTION

Gaseous ammonia (NH_3) is the predominant alkaline gas and the major form of reactive nitrogen in the atmosphere.[1] NH_3 is mainly emitted from indoor decorative materials containing urea or NH_3 compound-based antifreeze admixtures and outdoor agriculture and nonagricultural activities.[2] Excessive emission of NH_3 gives rise to a number of negative effects on human health and the environment. In particular, recent studies have suggested that NH_3 participates as NH_4^+ in the formation of secondary inorganic aerosol through the neutralization of HNO_3 and H_2SO_4, greatly contributing to the formation of urban haze.[1−4] Therefore, NH_3 is a key precursor for fine particle formation, and research on NH_3 emission control is currently attracting more and more attention.[5,6]

Photodegradation of gaseous pollutants has been widely studied in the area of environmental catalysis, such as in the removal of formaldehyde,[7,8] volatile organic compounds,[9,10] NO_x, and so forth.[11,12]Very recently, researchers have recognized the potential of TiO_2 in the photocatalytic elimination of NH_3 at room temperature.[13−15] Commercial and modified anatase TiO_2 show excellent activity for the removal of gaseous NH_3 under UV light.[15] We previously reported that TiO_2 with predominant exposure of {001} facets has superior activity for NH_3 oxidation compared to TiO_2 with {101} or {010} facets exposed and that there is a remarkable synergistic effect between {001} facets and the surface F ions on PCO of NH_3, while no such synergistic effect between {101} facets and the surface F ions exists.[16,17] Nevertheless, TiO_2 has a relatively large band gap (3.0−3.2 eV), which limits its application under visible light, and the photocatalytic oxidation (PCO) of NH_3 under visible light irradiation has not yet been achieved. Developing efficient visible-light-sensitive photocatalysts for the elimination of gaseous NH_3 is of great interest.

In principle, a visible-light-sensitive photocatalyst exploited for environmental purification should meet two requirements. First, such a photocatalyst should have a narrow enough band gap to allow visible light excitation, which is a necessary precondition.[18,19] Second, a suitable redox potential for the excited photocatalyst toward the target pollutant is indispensable, but this aspect is often neglected.[20,21] Nonmetal or metal-doped TiO_2, such as N-,[18] C-,[22] Fe-,[23] and Cu-doped TiO_2,[24,25] have been widely studied as the most common visible-light-sensitive photocatalysts. Because the dopant energy levels in these materials tend to be isolated above the valence band (VB) of TiO_2, the photoexcited holes in the dopant levels have less oxidation power and lower mobility as compared to holes in the VB of TiO_2.[18,26] Therefore, the main active species usually arise from the activation of O_2 via

Received: April 24, 2020
Revised: July 17, 2020
Accepted: July 31, 2020
Published: July 31, 2020

https://dx.doi.org/10.1021/acs.est.0c02589
Environ. Sci. Technol. 2020, 54, 10544−10550

photoexcited electrons in the conduction band (CB).[26,27] However, it should be noted that not all pollutants can be degraded if only O_2 molecules are activated, for example, the benzene series in volatile organic compounds (VOCs).[9] To the best of our knowledge, the previous studies on band modification of photocatalysts mainly focus on the reduction of the band gap to induce a visible light response,[19,28] while the influence of the redox potential of photoexcited holes and electrons on the pollutant oxidation has seldom been investigated or discussed.

In this work, we selected a set of typical semiconductor materials (N-TiO_2, g-C_3N_4, and Ag_3PO_4), which are common visible-light-sensitive photocatalysts, and tested and compared their activities in NH_3 oxidation. We interestingly observed that Ag_3PO_4 can harness visible light to oxidize NH_3, while TiO_2, N-TiO_2, and g-C_3N_4 exhibit no activity for NH_3 oxidation under the same conditions. Based on the characterization results of X-ray diffraction (XRD), Brunauer–Emmett–Teller (BET), electron paramagnetic resonance (EPR), and so forth, we reveal that along with a suitable band gap for visible light excitation, the redox potential of photoexcited holes in a photocatalyst plays a key role in the course of NH_3 oxidation. These findings are helpful for the design of visible-light-driven photocatalysts for gaseous NH_3 oxidation and provide a new insight into the PCO of pollutants.

2. EXPERIMENTAL SECTION

2.1. Synthesis of Catalysts. Ag_3PO_4 particles were prepared by an ion-exchange method using Na_2HPO_4 and $AgNO_3$ aqueous solutions, similar to previous reports.[29−31] In a typical experiment, 10 mL of Na_2HPO_4 aqueous solution (0.2 M) was added carefully to the prepared 10 mL of $AgNO_3$ aqueous solution (0.6 M), and the obtained golden yellow precipitate was carefully washed with deionized water several times and dried at 333 K. Graphitic carbon nitride (g-C_3N_4) was prepared by a pyrolysis method, in which melamine was heated at 550 °C for 4 h. A sol−gel method was employed to prepare N-TiO_2; tetrabutyl titanate was first dropped into the NH_4Cl solution, then the obtained gel was dried at 373 K, and finally, the gel was calcined in a muffle furnace at 773 K for 4 h. TiO_2 (P25, Degussa) was purchased from Sigma.

2.2. NH_3 Oxidation Activity Test. The setup for activity testing for NH_3 oxidation was a self-designed flow reactor. A round sample dish containing 0.1 g of photocatalyst powders was used to test the NH_3 oxidation activity. Commercial Xe lamp (500 W) was the light source. The light intensity was 10.2 mW/cm^2 when an optical filter (λ > 420 nm) was used. The concentrations of NH_3 were online detected by an FTIR spectrometer (Nicolet 380). The reactant gas was 50 ppm NH_3, 20 vol % O_2, and N_2 balance, and the relative humidity of the reactant gas was controlled about 50%. In a circular flow activity test experiment, the mixed gas was allowed to flow circularly through the reactor where the reactant gas volume was about 1.5 L and the flow was 50 mL/min.

2.3. Characterization Methods. An X'Pert PRO MPD X-ray powder diffractometer was applied to measure the XRD of the photocatalysts, in which Cu Kα radiation is operating at 40 kV and 40 mA. The UV−vis diffuse reflection spectroscopy (DRS) spectra were measured using a UV−vis spectrophotometer (U-3310, Hitachi). The morphology of the photocatalysts was investigated by a field emission scanning electron microscope (SU8000). The powdered samples were deposited on silicon wafers before field emission scanning electron microscopy measurements. The EPR spectra were recorded with a Bruker E500 EPR spectrometer. NH_3 was adsorbed on the samples to saturation before EPR measurements.

3. RESULTS AND DISCUSSION

TiO_2, N-TiO_2, g-C_3N_4, and Ag_3PO_4 are typical photocatalysts in the field of heterogeneous photocatalysis and can be easily synthesized by well-known procedures. Figure 1 and Figure 2 show the XRD patterns and typical SEM images of the samples. The TiO_2 and N-TiO_2 samples exhibit the standard anatase XRD pattern, and g-C_3N_4 shows its typical diffraction peaks at 27.5 and 13.0°, which can be indexed to the (002) and (100) planes of graphite-like carbon nitride.[19,29,30] The XRD pattern of Ag_3PO_4 shows the characteristic body-centered cubic structure (JCPDS no. 06-0505). As shown in Figure 2, TiO_2 and N-TiO_2 samples show nanoparticles with a diameter of 20−30 nm, and the Ag_3PO_4 sample consists of agglomerated spherical particles with a diameter of 200−400 nm with smooth surface, while the g-C_3N_4 sample displays a two-dimensional lamellar structure.

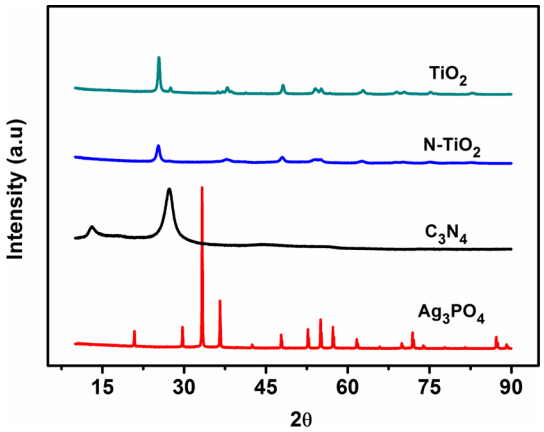

Figure 1. Powder XRD patterns of synthesized samples at room temperature.

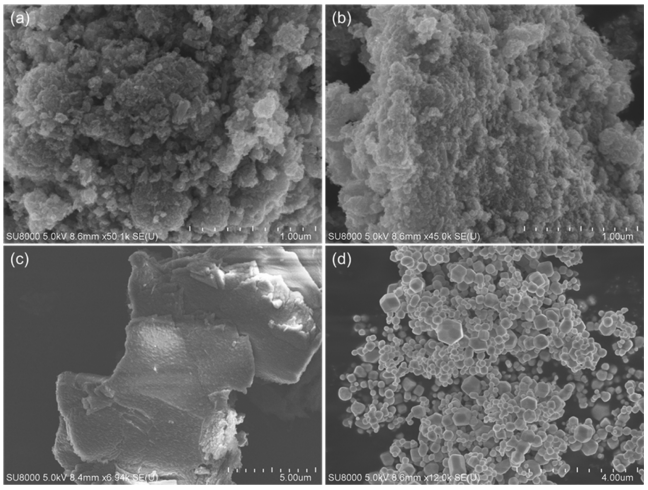

Figure 2. SEM images of (a) TiO_2, (b) N-TiO_2, (c) C_3N_4, and (d) Ag_3PO_4.

Visible light absorption is a crucial precondition for a visible-light-sensitive photocatalyst.[18,19,31,32] We measured and

https://dx.doi.org/10.1021/acs.est.0c02589
Environ. Sci. Technol. 2020, 54, 10544−10550

compared the UV−vis DRS spectra of the four samples. As displayed in Figure 3, the TiO_2 sample shows no observable

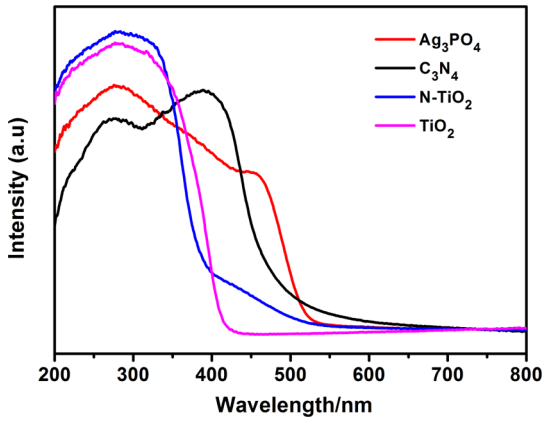

Figure 3. Diffuse reflectance spectra of the samples.

absorption in the visible light region because of its wide band gap (3.22 eV). In the case of N-TiO_2, the broad absorption in the visible region centered at about 450 nm is characteristic of the N-doped material. The absorption edge of the g-C_3N_4 sample is about 460 nm, which corresponds well with the band gap of pristine g-C_3N_4 (2.7 eV).[8] Ag_3PO_4 has a broader absorption in the visible region, with an absorption edge of around 530 nm. The band gap of Ag_3PO_4 was estimated to be 2.33 eV, consistent with previous studies.[33] Clearly, the as-synthesized photocatalysts, including N-TiO_2, g-C_3N_4, and Ag_3PO_4, have considerable visible absorption; hence, these three samples are potentially active for the PCO of NH_3 under visible light.

The samples were then tested for the PCO of gaseous NH_3 under visible light or simulated sunlight irradiation. The tests were performed in a flow reactor, where NH_3 continuously flowed over the photocatalysts at a constant inlet concentration. There was no activity in the absence of either the photocatalysts or light irradiation. As shown in Figure 4a, TiO_2, N-TiO_2, and g-C_3N_4 were not active for NH_3 oxidation under visible light, and no NH_3 conversion was detected. In contrast, we interestingly observed that Ag_3PO_4 shows a high efficiency for NH_3 oxidation with visible light irradiation, with the NH_3 conversion reaching about 70%. In the case of simulated sunlight irradiation (Figure 4b), TiO_2, N-TiO_2, and Ag_3PO_4 all showed considerable NH_3 conversion, with an activity order of Ag_3PO_4 > TiO_2 > N-TiO_2, while g-C_3N_4 was still inactive. The anatase TiO_2, as an efficient UV photocatalyst, showed no activity under visible light irradiation because it has no visible light absorption. N-TiO_2 or C_3N_4 has been reported to be active toward the degradation of organic dyes and some gaseous pollutants under visible light;[18,21,32] however, their quantum efficiencies are relatively low under visible light. It is possible that these materials displayed no activity in the flow reactor because of their low quantum efficiency. In order to exclude this factor, the samples were further tested in a circular flow mode under visible light irradiation, where the initial NH_3 concentration was 100 ppm and the reaction gases flowed over the photocatalysts in a circular fashion. As shown in Figure 5, the N-TiO_2 and C_3N_4 samples still showed no activity, while Ag_3PO_4 showed excellent NH_3 oxidation performance. Thus, it is clear that N-TiO_2 and C_3N_4 cannot oxidize NH_3 under visible light.

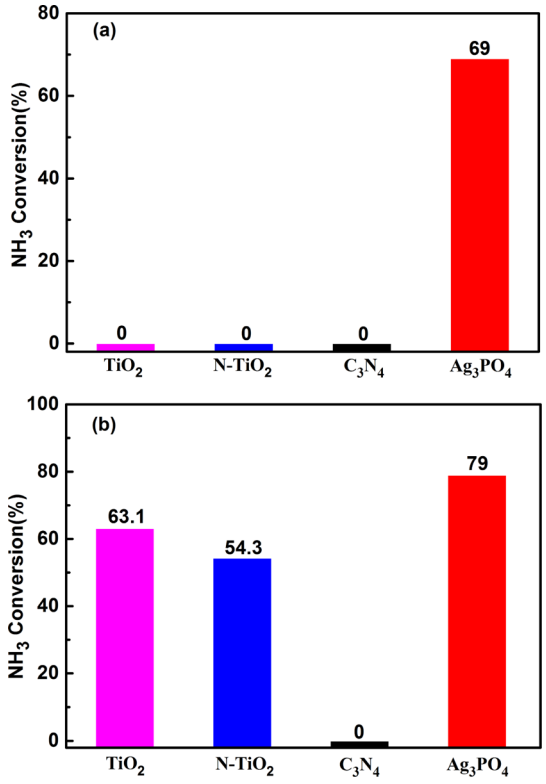

Figure 4. PCO of NH_3 over different samples under irradiation by visible light (a) and simulated sunlight (b) is compared.

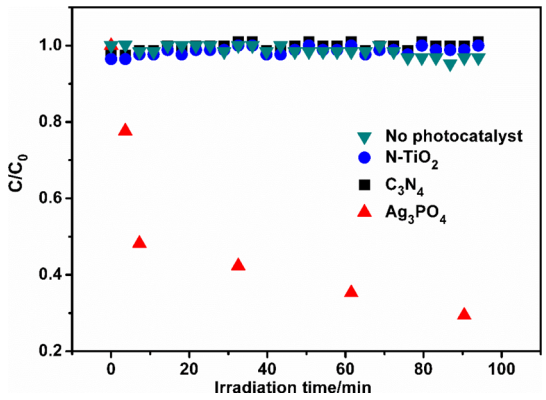

Figure 5. Cyclic activity tests of the PCO NH_3 over N-TiO_2, C_3N_4, and Ag_3PO_4 under visible light irradiation.

Many studies have revealed that photogenerated electrons can activate O_2 molecules to form reactive oxygen species, such as superoxide radical ($^{\bullet}O_2^-$), which then play important roles in photocatalysis.[21,22,34,35] Reactive oxygen species can be strongly trapped by 5,5-dimethyl-1-pyrroline *N*-oxide (DMPO) and then can be measured by EPR spectroscopy.[35] As shown in Figure 6b, in the case of N-TiO_2 and g-C_3N_4, DMPO−$^{\bullet}O_2^-$ species in acetonitrile dispersions were detected under visible light irradiation, which is a typical indication that O_2 molecules are activated by the photogenerated electrons on the surface of N-TiO_2 and g-C_3N_4, which is consistent with previous publications.[8,20] In contrast, no DMPO−$^{\bullet}O_2^-$ species were detected with the Ag_3PO_4 sample, indicating that O_2 cannot be activated by photogenerated electrons derived from the photoexcitation of Ag_3PO_4. In fact, the CB edge of Ag_3PO_4 is located at 0.45 eV,[33] providing an insufficient potential to

https://dx.doi.org/10.1021/acs.est.0c02589
Environ. Sci. Technol. 2020, 54, 10544−10550

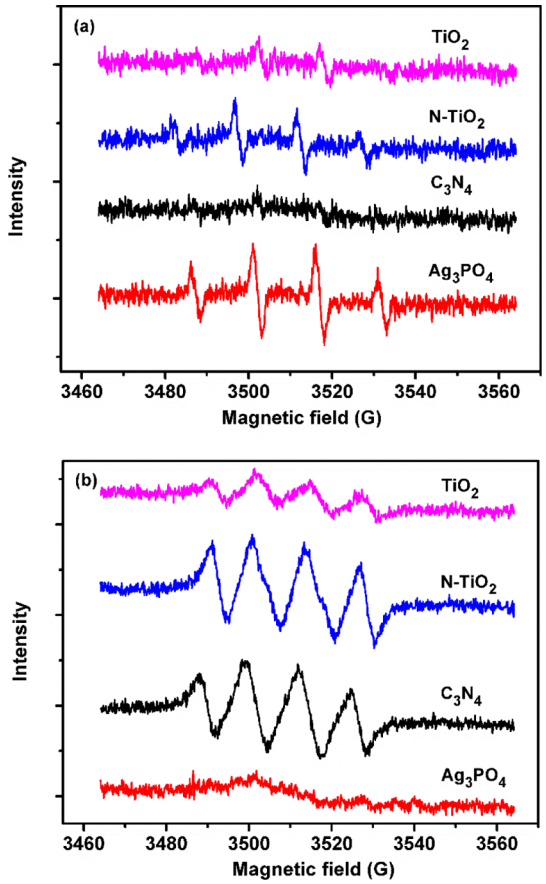

Figure 6. DMPO spin-trapping EPR spectra after 5 min visible irradiation in aqueous solutions (a) and acetonitrile solutions (b).

reduce O_2 to $^{\bullet}O_2^-$ ($E^{\circ}(O_2/^{\bullet}O_2^-) = -0.33$ V/NHE). Even though both N-TiO_2 and g-C_3N_4 can strongly activate O_2 molecules by providing abundant CB electrons, they exhibit no efficiency for NH_3 oxidation under visible light. By contrast, Ag_3PO_4 cannot activate O_2, but it shows high activity. These findings strongly refute the direct correlation between NH_3 oxidation and activation of O_2 molecules by CB electrons.

The dramatic redox potential differences of photoexcited holes in these semiconductors should be another crucial aspect with respect to their photocatalytic performance.[36−38] One possible pathway is that photogenerated holes initiate the production of hydroxyl radical ($^{\bullet}OH$) and trigger the indirect oxidation of NH_3. This indirect participation of holes is commonly involved in oxidation reactions of various reactants.[39−41] We therefore detected the amount of $^{\bullet}OH$ species produced by the samples under visible light. As shown in Figure 6a, four characteristic peaks of DMPO−$^{\bullet}OH$ adducts appear for N-TiO_2 and Ag_3PO_4 under visible light, indicating the formation of $^{\bullet}OH$. In contrast, no signal of DMPO−$^{\bullet}OH$ adducts is observed in the case of TiO_2 and g-C_3N_4 because visible light cannot excite TiO_2, and the VB holes (∼1.40 eV) from g-C_3N_4 are not capable of directly oxidizing OH^- or H_2O into $^{\bullet}OH$ radicals (1.99 eV for $OH^-/^{\bullet}OH$ and 2.37 eV for $H_2O/^{\bullet}OH$). Previous studies have shown that NH_3 oxidation by $^{\bullet}OH$ in solution is extremely slow because of the low reaction rate constant.[39,42] The N-TiO_2 sample here shows no activity for NH_3 oxidation under visible light, giving further evidence that $^{\bullet}OH$ is not kinetically suitable for the direct oxidation of NH_3. Hence, we can conclude that $^{\bullet}OH$ species do not play the key role in the PCO of NH_3.

The mechanism of the PCO of NH_3 over TiO_2 under UV irradiation has been investigated in previous studies.[13,14,43] It is proposed that the PCO of NH_3 follows a photo-iSCR mechanism on TiO_2, in which the first step is the activation of NH_3 to $^{\bullet}NH_2$, and $^{\bullet}NH_2$ then reacts with active oxygen species such as $^{\bullet}O_2^-$ and $^{\bullet}OH$ to generate the intermediate NO_x; finally, the in situ formed NO_x is reduced by $^{\bullet}NH_2$ to N_2

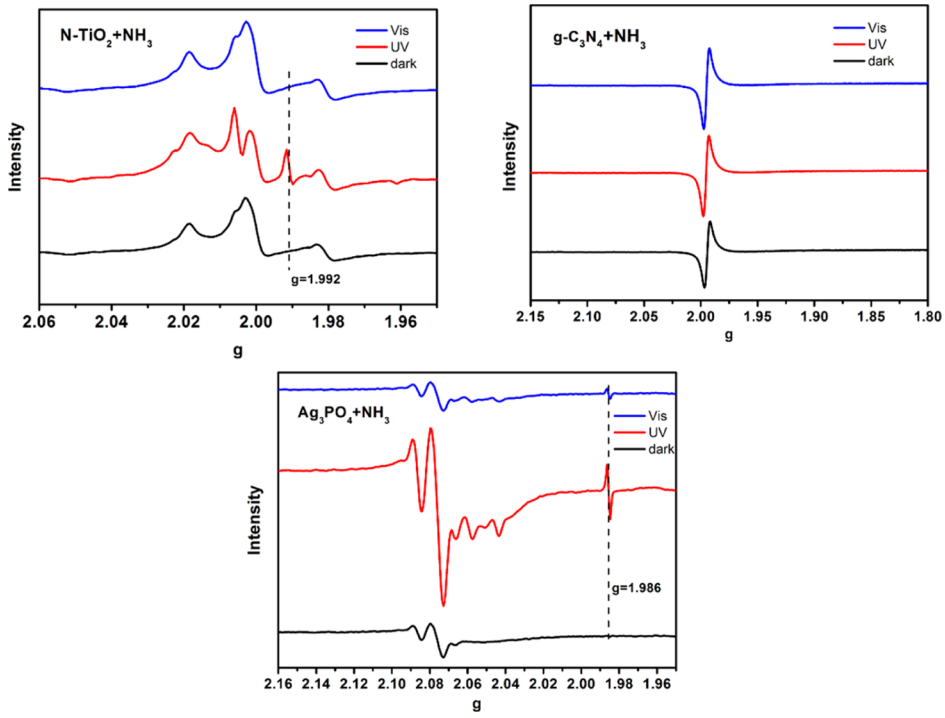

Figure 7. EPR spectra of N-TiO_2, C_3N_4, and Ag_3PO_4 after preadsorption of NH_3 at 90 K.

https://dx.doi.org/10.1021/acs.est.0c02589
Environ. Sci. Technol. 2020, 54, 10544−10550

or N_2O.[16,17] In addition, Yamazoe et al. confirmed the formation of $^{\bullet}NH_2$ on TiO_2 under UV irradiation by low-temperature EPR spectroscopy, and they suggested that the hole plays an important role in the activation of NH_3 to $^{\bullet}NH_2$. Based on these reports, we next performed EPR experiments at low temperature to investigate $^{\bullet}NH_2$ formation via the first step of NH_3 oxidation by holes over N-TiO_2, g-C_3N_4, and Ag_3PO_4 under visible light. As shown in Figure 7, the EPR signal remained unchanged over the NH_3 preadsorbed N-TiO_2 sample under visible light compared with that under dark conditions, while a new peak located in $g = 1.992$ due to $^{\bullet}NH_2$ formation appeared under UV irradiation,[13] indicating that the holes produced on N-TiO_2 under UV irradiation can oxidize the preabsorbed NH_3, while the holes excited by visible light cannot. In the case of g-C_3N_4, no change in EPR spectra was observed under UV or visible light, in accordance with its lack of activity for NH_3 oxidation. Ag_3PO_4 presents a peak located at $g = 1.986$ under visible light similar to that of N-TiO_2, indicating that the preadsorbed NH_3 is activated by holes to generate $^{\bullet}NH_2$. The EPR results of Ag_3PO_4 are in good agreement with the observation that Ag_3PO_4 has exceptional activity for NH_3 oxidation under both visible and UV light.

There is an essential question as to why the holes derived from N-TiO_2 and g-C_3N_4 under visible light cannot initiate the NH_3 oxidation, while the holes from N-TiO_2 and TiO_2 under UV light, and the holes from Ag_3PO_4 under visible or UV light, can trigger the NH_3 oxidation. Generally, the reactivity of holes is closely related to their oxidation capacity, while the oxidation capacity is dependent on the position of the VB. Hence, we can understand that the activity of samples for NH_3 oxidation is determined by their VB positions. The band structures of these four typical photocatalysts have been intensively investigated. As shown in Figure 8, the VB edges of

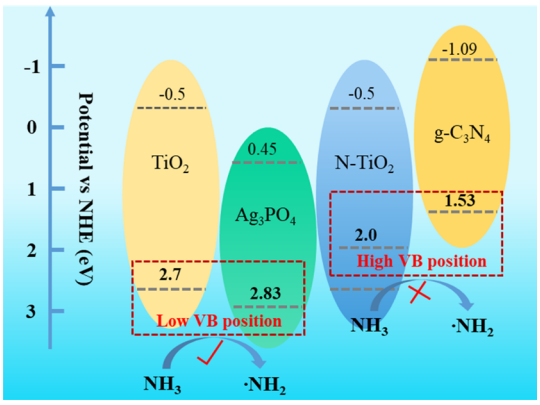

Figure 8. Band-edge positions of TiO_2, N-TiO_2, C_3N_4, and Ag_3PO_4.

TiO_2, C_3N_4, and Ag_3PO_4 are located at 2.7, 1.53, and 2.83 eV, respectively. As for N-TiO_2, the doped nitrogen energy levels are isolated above the VB of TiO_2 (located at about 2.0 eV). NH_3 oxidation did not occur on the surface of N-TiO_2 and g-C_3N_4 under visible light, implying that the redox potentials of photoexcited holes in the VB of N-TiO_2 and g-C_3N_4 are not sufficient for NH_3 oxidation. TiO_2 and Ag_3PO_4 have a low VB edge (below 2.7 eV) and exhibit exceptional activity for NH_3 oxidation, demonstrating that if the VB position of a photocatalyst is 2.7 eV or even lower, the holes are capable of NH_3 oxidation.

We have also prepared and tested other TiO_2-based materials such as metal- and nonmetal-doped TiO_2 (Fe, Cu, Ni, Co, C, and S) and noble metal (Pt and Pd)-modified TiO_2, and these materials all showed good activity under UV irradiation but no activity under visible light (Table S1). Generally, metal or nonmetal doping will reduce the band gap of TiO_2, causing the visible light absorption; however, the oxidation potential of holes in doped TiO_2 is lower compared with that in TiO_2, resulting in the decrease of oxidation ability. Further, we also prepared WO_3 which has a lower VB position. WO_3 showed activity for NH_3 oxidation under visible light (Figure S1), further proving that a low VB edge for activating NH_3 to $^{\bullet}NH_2$ is a crucial precondition.

We next carried out the DFT calculation about the thermodynamics of NH_3 to NH_2 ($NH_3 \rightarrow NH_2 + H$). This process is endothermic by about 113 kcal/mol, indicating that the N−H bond of NH_3 is difficult to be broken. The highest occupied molecular orbital (HOMO) and lowest unoccupied molecular orbital (LUMO) of NH_3 were also calculated by using Gaussian, and the results are shown in Table S2. The HOMO of NH_3 is −7.35 eV (about 2.85 eV vs NHE), which is very close to the VBs of TiO_2 and Ag_3PO_4 but far below the VBs of N-TiO_2 and g-C_3N_4, revealing that the HOMO electron of NH_3 tends to transfer to the excited VB of TiO_2 and Ag_3PO_4 associated with NH_3 activation to NH_2, while it cannot transfer to the excited VB of N-TiO_2 and g-C_3N_4.

On the basis of the above results and discussion, we now have an essential insight into the visible light PCO of NH_3. As for Ag_3PO_4, photoexcited electron−hole pairs can be produced under visible light irradiation because of its narrow band gap, the charges migrate to the surface of Ag_3PO_4, and the holes with high enough redox potential then activate NH_3 to form $^{\bullet}NH_2$ and initiate the reaction. In contrast, despite the fact that N-TiO_2 and g-C_3N_4 can also be photoexcited under visible light, NH_3 cannot be activated because of their poor oxidizing capacities associated with their high VB position. Additionally, it is noted that even though the active oxygen species such as $^{\bullet}O_2^-$ and $^{\bullet}OH$ can trigger NH_3 oxidation, they participate in subsequent reactions such as the formation of the intermediate NO_x, as proposed by Yamazoe et al.[14] and Kebede et al.[44,45]

4. CONCLUSIONS

In this work, we compared the performance of a set of typical semiconductors (Ag_3PO_4, TiO_2, N-TiO_2, and g-C_3N_4) in the PCO of NH_3 under visible light or simulated sunlight. We discovered that the semiconductor Ag_3PO_4 is an efficient visible-light-sensitive photocatalyst for the PCO of NH_3. Based on activity testing and EPR results, we confirmed that the first and also the key step in the PCO of NH_3 is NH_3 conversion into $^{\bullet}NH_2$, which is determined by the redox potential of photogenerated holes. We finally concluded that an effective visible-light-sensitive photocatalyst for NH_3 oxidation requires both a suitable band gap for visible light response and a low enough VB edge for NH_3 activation to $^{\bullet}NH_2$. These findings provide new insights into the PCO reaction of gaseous NH_3 and will contribute to the design of more efficient photocatalysts for NH_3 oxidation under visible light.

■ ASSOCIATED CONTENT

Supporting Information

The Supporting Information is available free of charge at https://pubs.acs.org/doi/10.1021/acs.est.0c02589.

https://dx.doi.org/10.1021/acs.est.0c02589
Environ. Sci. Technol. 2020, 54, 10544−10550

Synthesis of TiO_2-based materials; DFT calculation parameters; activity for PCO of NH_3 on WO_3 and TiO_2-based materials; and calculated results about LUMO and HOMO of NH_3 (PDF)

■ AUTHOR INFORMATION

Corresponding Author

Changbin Zhang − *State Key Joint Laboratory of Environment Simulation and Pollution Control, Research Center for Eco-Environmental Sciences, Chinese Academy of Sciences, Beijing 100085, China; University of Chinese Academy of Sciences, Beijing 100049, China;* orcid.org/0000-0003-2124-0620; Email: cbzhang@rcees.ac.cn

Authors

Min Chen − *State Key Joint Laboratory of Environment Simulation and Pollution Control, Research Center for Eco-Environmental Sciences, Chinese Academy of Sciences, Beijing 100085, China*

Hong He − *State Key Joint Laboratory of Environment Simulation and Pollution Control, Research Center for Eco-Environmental Sciences, Chinese Academy of Sciences, Beijing 100085, China; University of Chinese Academy of Sciences, Beijing 100049, China*

Complete contact information is available at: https://pubs.acs.org/10.1021/acs.est.0c02589

Notes

The authors declare no competing financial interest.

■ ACKNOWLEDGMENTS

This work was financially supported by the National Key R&D Program of China (2017YFC0211802) and the National Natural Science Foundation of China (21906174, 21976196, and 21936005).

■ REFERENCES

(1) Fu, X.; Wang, S.; Xing, J.; Zhang, X.; Wang, T.; Hao, J. Increasing ammonia concentrations reduce the effectiveness of particle pollution control achieved via SO_2 and NOx emissions reduction in East China. *Environ. Sci. Technol. Lett.* **2017**, *4*, 221−227.

(2) Chang, Y.; Zou, Z.; Zhang, Y.; Deng, C.; Hu, J.; Shi, Z.; Dore, A. J.; Collett, J. L., Jr. Assessing contributions of agricultural and nonagricultural emissions to atmospheric ammonia in a Chinese megacity. *Environ. Sci. Technol.* **2019**, *53*, 1822−1833.

(3) Kong, L.; Tang, X.; Zhu, J.; Wang, Z.; Pan, Y.; Wu, H.; Wu, L.; Wu, Q.; He, Y.; Tian, S.; Xie, Y.; Liu, Z.; Sui, W.; Han, L.; Carmichael, G. Improved inversion of monthly ammonia emissions in china based on the Chinese ammonia monitoring network and ensemble Kalman filter. *Environ. Sci. Technol.* **2019**, *53*, 12529−12538.

(4) Wu, L.; Ren, H.; Wang, P.; Chen, J.; Fang, Y.; Hu, W.; Ren, L.; Deng, J.; Song, Y.; Li, J.; Sun, Y.; Wang, Z.; Liu, C.-Q.; Ying, Q.; Fu, P. Aerosol ammonium in the urban boundary layer in Beijing: Insights from nitrogen isotope ratios and simulations in summer 2015. *Environ. Sci. Technol. Lett.* **2019**, *6*, 389−395.

(5) Wang, F.; He, G.; Zhang, B.; Chen, M.; Chen, X.; Zhang, C.; He, H. Insights into the activation effect of H_2 pretreatment on Ag/Al_2O_3 catalyst for the selective oxidation of ammonia. *ACS Catal.* **2019**, *9*, 1437−1445.

(6) Wang, F.; Ma, J.; He, G.; Chen, M.; Zhang, C.; He, H. Nanosize effect of Al_2O_3 in Ag/Al_2O_3 catalyst for the selective catalytic oxidation of ammonia. *ACS Catal.* **2018**, *8*, 2670−2682.

(7) Zhu, X.; Jin, C.; Li, X.-S.; Liu, J.-L.; Sun, Z.-G.; Shi, C.; Li, X.; Zhu, A.-M. Photocatalytic formaldehyde oxidation over plasmonic Au/TiO_2 under visible light: Moisture indispensability and light enhancement. *ACS Catal.* **2017**, *7*, 6514−6524.

(8) Song, S.; Lu, C.; Wu, X.; Jiang, S.; Sun, C.; Le, Z. Strong base g-C_3N_4 with perfect structure for photocatalytically eliminating formaldehyde under visible-light irradiation. *Appl. Catal., B* **2018**, *227*, 145−152.

(9) Debono, O.; Hequet, V.; Le Coq, L.; Locoge, N.; Thevenet, F. Voc ternary mixture effect on ppb level photocatalytic oxidation: Removal kinetic, reaction intermediates and mineralization. *Appl. Catal., B* **2017**, *218*, 359−369.

(10) Héquet, V.; Raillard, C.; Debono, O.; Thévenet, F.; Locoge, N.; Le Coq, L. Photocatalytic oxidation of VOCs at ppb level using a closed-loop reactor: The mixture effect. *Appl. Catal., B* **2018**, *226*, 473−486.

(11) Ma, J.; He, H.; Liu, F. Effect of fe on the photocatalytic removal of nox over visible light responsive Fe/TiO_2 catalysts. *Appl. Catal., B* **2015**, *179*, 21−28.

(12) Ma, J.; Wu, H.; Liu, Y.; He, H. Photocatalytic removal of NO_x over visible light responsive oxygen-deficient TiO_2. *J. Phys. Chem. C* **2014**, *118*, 7434−7441.

(13) Yamazoe, S.; Okumura, T.; Hitomi, Y.; Shishido, T.; Tanaka, T. Mechanism of photo-oxidation of NH_3 over TiO_2: Fourier transform infrared study of the intermediate species. *J. Phys. Chem. C* **2007**, *111*, 11077−11085.

(14) Yamazoe, S.; Teramura, K.; Hitomi, Y.; Shishido, T.; Tanaka, T. Visible light absorbed NH_2 species derived from NH_3 adsorbed on TiO_2 for photoassisted selective catalytic reduction. *J. Phys. Chem. C* **2007**, *111*, 14189−14197.

(15) Heylen, S.; Smet, S.; Laurier, K. G. M.; Hofkens, J.; Roeffaers, M. B. J.; Martens, J. A. Selective photocatalytic oxidation of gaseous ammonia to dinitrogen in a continuous flow reactor. *Catal. Sci. Technol.* **2012**, *2*, 1802−1805.

(16) Chen, M.; Ma, J.; Zhang, B.; He, G.; Li, Y.; Zhang, C.; He, H. Remarkable synergistic effect between {001} facets and surface f ions promoting hole migration on anatase TiO_2. *Appl. Catal., B* **2017**, *207*, 397−403.

(17) Chen, M.; Ma, J.; Zhang, B.; Wang, F.; Li, Y.; Zhang, C.; He, H. Facet-dependent performance of anatase TiO_2 for photocatalytic oxidation of gaseous ammonia. *Appl. Catal., B* **2018**, *223*, 209−215.

(18) Asahi, R.; Morikawa, T.; Irie, H.; Ohwaki, T. Nitrogen-doped titanium dioxide as visible-light-sensitive photocatalyst: Designs, developments, and prospects. *Chem. Rev.* **2014**, *114*, 9824−9852.

(19) Liu, G.; Yang, H. G.; Pan, J.; Yang, Y. Q.; Lu, G. Q.; Cheng, H.-M. Titanium dioxide crystals with tailored facets. *Chem. Rev.* **2014**, *114*, 9559−9612.

(20) Low, J.; Cheng, B.; Yu, J. Surface modification and enhanced photocatalytic CO_2 reduction performance of TiO_2: A review. *Appl. Surf. Sci.* **2017**, *392*, 658−686.

(21) Xu, H.; Ouyang, S.; Liu, L.; Reunchan, P.; Umezawa, N.; Ye, J. Recent advances in TiO_2-based photocatalysis. *J. Mater. Chem. A* **2014**, *2*, 12642−12661.

(22) Ceotto, M.; Lo Presti, L.; Cappelletti, G.; Meroni, D.; Spadavecchia, F.; Zecca, R.; Leoni, M.; Scardi, P.; Bianchi, C. L.; Ardizzone, S. About the nitrogen location in nanocrystalline N-doped TiO_2: Combined DFT and EXAFS approach. *J. Phys. Chem. C* **2012**, *116*, 1764−1771.

(23) Zhang, H.; Wang, W.; Zhao, H.; Zhao, L.; Gan, L.-Y.; Guo, L.-H. Facet-dependent interfacial charge transfer in Fe (III)-grafted TiO_2 nanostructures activated by visible light. *ACS Catal.* **2018**, *8*, 9399−9407.

(24) Unwiset, P.; Makdee, A.; Chanapattharapol, K. C.; Kidkhunthod, P. Effect of Cu addition on TiO_2 surface properties and photocatalytic performance: X-ray absorption spectroscopy analysis. *J. Phys. Chem. Solids* **2018**, *120*, 231−240.

(25) Šuligoj, A.; Arčon, I.; Mazaj, M.; Dražić, G.; Arčon, D.; Cool, P.; Štangar, U. L.; Tušar, N. N. Surface modified titanium dioxide using transition metals: Nickel as a winning transition metal for solar light photocatalysis. *J. Mater. Chem. A* **2018**, *6*, 9882−9892.

(26) Liu, F.; Feng, N.; Wang, Q.; Xu, J.; Qi, G.; Wang, C.; Deng, F. Transfer channel of photoinduced holes on a TiO_2 surface as revealed by solid-state nuclear magnetic resonance and electron spin resonance spectroscopy. *J. Am. Chem. Soc.* **2017**, *139*, 10020−10028.
(27) Li, H.; Shang, H.; Cao, X.; Yang, Z.; Ai, Z.; Zhang, L. Oxygen vacancies mediated complete visible light no oxidation via side-on bridging superoxide radicals. *Environ. Sci. Technol.* **2018**, *52*, 8659−8665.
(28) Ge, M.; Cao, C.; Huang, J.; Li, S.; Chen, Z.; Zhang, K.-Q.; Al-Deyab, S. S.; Lai, Y. A review of one-dimensional TiO_2 nanostructured materials for environmental and energy applications. *J. Mater. Chem. A* **2016**, *4*, 6772−6801.
(29) Yu, Y.; Yang, X.; Zhao, Y.; Zhang, X.; An, L.; Huang, M.; Chen, G.; Zhang, R. Engineering the band gap states of the rutile TiO_2 (110) surface by modulating the active heteroatom. *Angew. Chem., Int. Ed.* **2018**, *57*, 8550−8554.
(30) Liu, W.; Zhang, L.; Liu, X.; Liu, X.; Yang, X.; Miao, S.; Wang, W.; Wang, A.; Zhang, T. Discriminating catalytically active fenx species of atomically dispersed Fe-N-C catalyst for selective oxidation of the c-h bond. *J. Am. Chem. Soc.* **2017**, *139*, 10790−10798.
(31) Fujiwara, K.; Müller, U.; Pratsinis, S. E. Pd subnano-clusters on TiO_2 for solar-light removal of no. *ACS Catal.* **2016**, *6*, 1887−1893.
(32) Fu, H.; Pan, C.; Yao, W.; Zhu, Y. Visible-light-induced degradation of rhodamine b by nanosized Bi_2WO_6. *J. Phys. Chem. B* **2005**, *109*, 22432−22439.
(33) Bi, Y.; Ouyang, S.; Umezawa, N.; Cao, J.; Ye, J. Facet effect of single-crystalline Ag_3PO_4 sub-microcrystals on photocatalytic properties. *J. Am. Chem. Soc.* **2011**, *133*, 6490−6492.
(34) Chen, C.; Ma, W.; Zhao, J. Semiconductor-mediated photodegradation of pollutants under visible-light irradiation. *Chem. Soc. Rev.* **2010**, *39*, 4206−4219.
(35) Xiao, J.; Rabeah, J.; Yang, J.; Xie, Y.; Cao, H.; Brückner, A. Fast electron transfer and (OH)-O-center dot formation: Key features for high activity in visible-light-driven ozonation with C_3N_4 catalysts. *ACS Catal.* **2017**, *7*, 6198−6206.
(36) Chen, Z.; Mitchell, S.; Vorobyeva, E.; Leary, R. K.; Hauert, R.; Furnival, T.; Ramasse, Q. M.; Thomas, J. M.; Midgley, P. A.; Dontsova, D.; Antonietti, M.; Pogodin, S.; Lopez, N.; Perez-Ramirez, J. Stabilization of single metal atoms on graphitic carbon nitride. *Adv. Funct. Mater.* **2017**, *27*, 1605785.
(37) Zhang, Z.; Zhu, Y.; Chen, X.; Zhang, H.; Wang, J. A full-spectrum metal-free porphyrin supramolecular photocatalyst for dual functions of highly efficient hydrogen and oxygen evolution. *Adv. Mater.* **2019**, *31*, 1806626.
(38) Zhang, M.; Xu, J.; Zong, R.; Zhu, Y. Enhancement of visible light photocatalytic activities via porous structure of g-C_3N_4. *Appl. Catal., B* **2014**, *147*, 229−235.
(39) Huang, L.; Li, L.; Dong, W.; Liu, Y.; Hou, H. Removal of ammonia by oh radical in aqueous phase. *Environ. Sci. Technol.* **2008**, *42*, 8070−8075.
(40) Wang, Y.; Zhao, X.; Cao, D.; Wang, Y.; Zhu, Y. Peroxymonosulfate enhanced visible light photocatalytic degradation bisphenol a by single-atom dispersed ag mesoporous g-C_3N_4 hybrid. *Appl. Catal., B* **2017**, *211*, 79−88.
(41) Yang, W.; Zhu, Y.; You, F.; Yan, L.; Ma, Y.; Lu, C.; Gao, P.; Hao, Q.; Li, W. Insights into the surface-defect dependence of molecular oxygen activation over birnessite-type MnO_2. *Appl. Catal., B* **2018**, *233*, 184−193.
(42) Ji, Y.; Luo, Y. First-principles study on the mechanism of photoselective catalytic reduction of no by NH_3 on anatase TiO_2 (101) surface. *J. Phys. Chem. C* **2014**, *118*, 6359−6364.
(43) Yamazoe, S.; Okumura, T.; Tanaka, T. Photo-oxidation of NH_3 over various TiO_2. *Catal. Today* **2007**, *120*, 220−225.
(44) Kebede, M. A.; Scharko, N. K.; Appelt, L. E.; Raff, J. D. Formation of nitrous acid during ammonia photooxidation on TiO_2 under atmospherically relevant conditions. *J. Phys. Chem. Lett.* **2013**, *4*, 2618−2623.
(45) Kebede, M. A.; Varner, M. E.; Scharko, N. K.; Gerber, R. B.; Raff, J. D. Photooxidation of ammonia on TiO_2 as a source of no and NO_2 under atmospheric conditions. *J. Am. Chem. Soc.* **2013**, *135*, 8606−8615.

https://dx.doi.org/10.1021/acs.est.0c02589
Environ. Sci. Technol. 2020, 54, 10544−10550